Journal of Materials Chemistry C

ROYAL SOCIETY OF CHEMISTRY

PAPER

View Article Online
View Journal

Cite this: DOI: 10.1039/d4tc00386a

Unveiling symmetry: a comparative analysis of asymmetric and symmetric non-fullerene acceptors in organic solar cells†

Rudranarayan Khatua and Anirban Mondal *

Received 26th January 2024,
Accepted 29th March 2024

DOI: 10.1039/d4tc00386a

rsc.li/materials-c

This study investigates the design and analysis of symmetric and asymmetric non-fullerene acceptors (NFAs), focusing on the burgeoning interest in asymmetric NFAs due to their exceptional solar cell properties. Our approach involves modifying the core and introducing two distinct terminal end-groups to the π-core system. Through rigorous first-principle simulations, we systematically explore the solar cell parameters of the designed NFAs when combined with a PM6 polymer. Surprisingly, our results demonstrate that incorporating an A5 acceptor, alongside other end-group acceptors (A1–A5), leads to a significant increase in the difference between ground and excited dipole moments ($\Delta\mu$), enhanced charge separation rates (k_{CS}), and notably reduced energy losses (<0.35 eV) compared to other complexes. Furthermore, our findings challenge the conventional wisdom that asymmetric compounds consistently outperform symmetric ones. We identify specific symmetric configurations, particularly those paired with A5 acceptors that exhibit substantial improvements in solar cell properties. This study emphasizes the critical importance of thoughtful material design, providing valuable insights for researchers striving to develop next-generation small-molecule acceptors for organic solar cells.

1 Introduction

Significant achievements in organic solar cells (OSCs) have been noticed in the last few years due to the rapid growth of non-fullerene acceptors (NFAs) over fullerene-based acceptors.[1–5] It is worth noting that the power conversion efficiency (PCE) of NFA-based organic solar cells remains below that of their inorganic perovskite counterparts, which can achieve efficiencies as high as 25.7%.[6,7] This discrepancy in PCEs is attributed primarily to the high non-radiative recombination loss in NFAs. Thus, it is a crucial challenge for the researcher to design a high-quality active layer (molecular stacking of a donor and acceptor blend) to reduce the non-radiative recombination loss without affecting charge separation and transport. Typically, the active layer consists of polymer donor and acceptor materials, which are of A–D–A, A–DA′D–A, and A–D–A′–D–A types, where A and A′ represent the terminal acceptor unit and core acceptor unit, respectively, and D refers to the core donor unit. In general, similar acceptor units fuzed at the terminal position result in a symmetrical acceptor, whereas incorporation of unequal acceptor units leads to an asymmetric one. Currently, the PCEs of the Y-series (A–DA′D–A-type) based NFAs are over 19%.[8–10] Symmetrical small-molecule acceptors designed with the A–D–A or A–DA′D–A configuration exhibit remarkable photophysical applications.[11–15] This remarkable progress has significantly advanced the prospects of commercializing organic solar cells.

Due to their breakthrough efficiencies, asymmetric non-fullerene acceptors have drawn considerable attention in organic solar cell applications.[16–19] Asymmetric or symmetry-breaking non-fullerene acceptors are designed with asymmetric core units, side chains, and terminal groups.[20–22] Moreover, an asymmetric terminal acceptor group-based complex consists of two unequal acceptors (A1 and A2), which are fuzed at the end positions of the complex.[23,24] Terminal acceptors can be classified into two types based on their performances to yield a high J_{SC} (short-circuit current density) and (or) a high V_{OC} (open-circuit voltage). The effective combination of a terminal group exhibiting a high J_{SC} and another terminal group with a substantial V_{OC} has successfully minimized energy losses, consequently enhancing power conversion efficiencies, as reported by Liu *et al.*[20] In a comparative analysis between symmetric and asymmetric complexes, it is reported by Gopikrishna *et al.* that introducing asymmetry to the terminal acceptor of the IPC-BEH-IC2F complex resulted in a power conversion efficiency of 12.70%, surpassing the efficiencies of the symmetrical

Department of Chemistry, Indian Institute of Technology Gandhinagar, Gujarat, 382355, India. E-mail: amondal@iitgn.ac.in

† Electronic supplementary information (ESI) available: Optimized structures and molecular orbitals of donor–acceptor complex, electrostatic potential surfaces, variation in the rates of charge separation and recombination, energy loss *versus* dipole moment differences, heat map plots, tables of electronic and photophysical parameters. See DOI: https://doi.org/10.1039/d4tc00386a

acceptors IPC-BEH-IPC (7.26%) and IC2F-BEH-IC2F (11.05%) when blended with a PBDB-T polymer.[19] A balanced open-circuit voltage and short-circuit current is observed in the asymmetric compound IPC-BEH-IC2F, which lies in between the two symmetrical acceptors IPC-BEH-IPC and IC2F-BEH-IC2F. In recent years, numerous research groups have demonstrated asymmetric NFAs consisting of A–D–A, A–DA′D–A, and A–D–A′–D–A type configurations with breakthrough efficiencies.[18,25,26] Sun *et al.* reported an asymmetric IDTT-2F-Th compound (fuzed with different terminal end-groups, TIC and 2FIC); when blended with a PBT1-C-2Cl polymer, it exhibited a remarkable PCE exceeding 12%.[27] Bo *et al.* synthesized an A–D–A type asymmetric compound a-IT-2OM, which exhibited a device efficiency of 12.07%, when blended with a PBDB-T polymer.[28] Luo and coworkers analyzed asymmetric derivatives of BTP-2F-ThCl by introducing IC2F and ThCl as terminal acceptors. BTP-2F-ThCl blended with PM6 yielded a remarkable PCE of 17.06%.[29] The increase in PCE was attributed to the simultaneous enhancements in both V_{OC} and J_{SC} compared to those of BTP-4F (16.37%) and BTP-2ThCl (14.49%) complexes. These findings suggest that utilizing asymmetric molecules holds significant promise for designing highly efficient active layer materials.

While the existing literature highlights the significant strides made in optimizing short-circuit current and open-circuit voltage through the incorporation of distinct terminal acceptor groups, there exist noteworthy loopholes and gaps that necessitate further exploration. The reported successes in PCE improvements, such as the 12.70% achieved by the IPC-BEH-IC2F complex, underscore the potential of asymmetric NFAs. However, a comprehensive understanding of the underlying molecular interactions, energy transfer mechanisms, and structure–property relationships is crucial for further advancements in this field. Computational modeling emerges as an indispensable tool in unraveling these complexities, allowing for a more precise and predictive approach to designing and optimizing asymmetric NFAs. By leveraging computational simulations, it is possible to explore diverse molecular configurations, predict performance outcomes, and guide the synthesis of novel asymmetric NFAs with enhanced efficiencies. Bridging these computational insights with experimental validations will pave the way for overcoming current limitations and unlocking the full potential of asymmetric NFAs in organic solar cell applications.

This study introduces a novel material design approach to explore symmetric and asymmetric non-fullerene acceptors. By combining five distinct acceptor units and four core donor units, as referenced in previous works (ref. 30–37), we systematically constructed acceptor–donor–acceptor (A*X*–D*Y*–A*X*) configurations, where *X* and *Y* denote acceptor units 1–5 and core units 1–4, respectively. Commencing with a single core unit (D1) and five terminal acceptors (A1–A5), we generated fifteen NFAs by varying the terminal acceptor units while maintaining a fixed core unit (D1). This systematic approach yielded ten asymmetric and five symmetric compounds. By replicating the procedure for other core units (D2–D4) functionalized with the same terminal acceptor units (A1–A5), we obtained 15 symmetric and 30 asymmetric NFAs. Quantum chemical calculations, employing the density functional theory (DFT) and time-dependent DFT (TD-DFT) methods, were utilized to compute the solar cell properties of the designed systems. This comprehensive exploration of symmetric and asymmetric NFAs provides a solid foundation for our subsequent computational investigations into their electronic and optical properties, enabling a deeper understanding and optimization of these materials for enhanced solar cell performance.

2 Methods

2.1 Computational details

We have meticulously tested the performance of three different DFT functionals, M06-2X,[38] CAM-B3LYP,[39–41] and dispersion-corrected B3LYP (B3LYP-D3) combined with a Def2-SVP basis set. The computed absorption wavelengths of the complexes A1–D1–A1, A2–D2–A2, A1–D3–A1, and A2–D4–A2 obtained from those three different levels of theory are summarized and compared against the available experimental measurements in Table S1 of the ESI.† Among the tested variations, the B3LYP-D3/Def2-SVP level of theory shows the best agreement with the experimental measurements. Thus, we considered the same level of theory to compute the electronic and photovoltaic properties of the NFA complexes investigated in this study. The ground geometries were optimized using the B3LYP-D3 dispersion-corrected hybrid functional[42] and the Def2-SVP basis set.[43] Global minima of the optimized geometry were confirmed through frequency analysis where any imaginary frequencies were absent. Both ground and excited-state calculations were carried out at the same level of theory, considering chloroform ($CHCl_3$, ε = 4.7713) as the solvent using the conductor-like polarizable continuum model (CPCM) as implemented in the Gaussian 09 program.[44] Photophysical parameters such as the transition dipole moment along the major axis (μ_{tr}), vertical excitation energy corresponding to the transition from S_0 to S_1, and polarizability of the donor–acceptor (D/A) complexes were estimated at the B3LYP-D3/Def2-SVP level of theory using the ORCA package, v.5.0.[45] A monomer unit of the PM6 polymer was used as the donor that was combined with the designed NFAs to investigate the donor–acceptor interface properties.

The Conformer-Rotamer Ensemble Sampling Tool (CREST) was used for conformational searching calculations of the D/A complex.[46] The semi-empirical tight binding method GFN-xTB was used to perform the abovementioned calculations using the xTB program.[46,47] The conformational search algorithm iMTD-GC has been implemented in CREST to conduct metadynamics (MTD) simulations.[47] MTD simulations were performed with specified sampling settings: a total simulation time of 200 ps, a time scale of 5.0 fs, a trajectory dump step of 100 fs, and a bias potential dump step of 1.0 ps. We utilized the module above to generate hundreds of conformers for each D/A complex. To further estimate the electronic couplings of the D/A complexes, we selected a maximum of ten D/A π-stacked conformers, in which five conformers, each lying energetically

highest and lowest in the potential energy surface, were chosen. This step yielded 600 conformers derived from 60 asymmetric and symmetric variations of designed NFAs.

The rates of charge separation (CS) and charge recombination (CR) at the donor–acceptor interface were evaluated within the hopping transport formalism.[48,49]

$$k = \frac{|V_{DA}|^2}{\hbar}\sqrt{\frac{\pi}{\lambda k_B T}}\exp\left[-\frac{(\Delta G - \lambda)^2}{4\lambda k_B T}\right] \quad (1)$$

Here, V_{DA} is the electronic coupling of the D/A complex, k_B is the Boltzmann constant, ΔG is the free energy change during the charge separation or recombination process (ΔG_{CS} or ΔG_{CR}), and λ is the reorganization energy. The electronic coupling of the selected D/A complexes was estimated using a generalized Mulliken–Hush model:[50]

$$V_{DA} = \frac{\mu_{tr}\Delta E}{\sqrt{(\Delta\mu)^2 + 4(\mu_{tr})^2}} \quad (2)$$

Here, μ_{tr} is the transition dipole moment along the major axis, ΔE is the vertical excitation energy transition from the ground state (S_0) to the first excited state (S_1), and $\Delta\mu$ is the dipole moment difference between the S_0 and S_1 states of the D/A complex. $\Delta\mu$ of the complex was estimated using the finite model.[50]

$$E_{exe}(F) = E_{exe}(0) - \Delta\mu F - \frac{1}{2}\Delta\alpha F^2 \quad (3)$$

Here, F denotes the external electric field set to 10^{-4} a.u., $E_{exe}(0) = \Delta E$ is the excitation energy at zero fields of the D/A complexes, and $\Delta\alpha$ defines the difference in polarizability between the D/A complexes in the presence and in the absence of an external electric field. The free energy change during charge recombination (ΔG_{CR}) and charge separation (ΔG_{CS}) was evaluated using eqn (4) and (5):[2,50,51]

$$\Delta G_{CR} = E^{D}_{HOMO} - E^{A}_{LUMO} \quad (4)$$

$$\Delta G_{CS} = -\Delta G_{CR} - E_{OP} \quad (5)$$

where E^{D}_{HOMO} denotes the HOMO of the donor, E^{A}_{LUMO} is the LUMO of the acceptor, and E_{OP} is the first excitation energy transition from S_0 to S_1 of the free base donor. It was estimated as $1240/\lambda_{max}$.

The total reorganization energy (λ) comprises two parts: inner reorganization energy (λ_i) and external reorganization energy (λ_s). The λ_i value was determined independently through the geometry relaxation in the donor polymer (λ_h) and non-fullerene acceptors (λ_e) during the charge transfer processes. The external reorganization energy was set to 0.3 eV.[51] The four-point method was employed to estimate the internal reorganization energy of the D/A complexes.

$$\lambda = \lambda_i + \lambda_s \quad (6)$$

$$\lambda_i = \lambda_h + \lambda_e \quad (7)$$

$$\lambda_h = (E^{C}_{n} - E^{N}_{n}) + (E^{N}_{c} - E^{C}_{c}) \quad (8)$$

$$\lambda_e = (E^{A}_{n} - E^{N}_{n}) + (E^{N}_{a} - E^{A}_{a}) \quad (9)$$

Here, the subscript indicates the charge state and the superscript indicates the molecule's geometry.

The exciton binding energy (E_b) of an NFA defines the energy required to separate the coulombically bound electron and hole pair and is computed using eqn (10):[52]

$$E_b = |E_{HOMO\text{–}LUMO}| - E_{OP} \quad (10)$$

where E_{OP} is the excitation energy ($S_0 \rightarrow S_1$) of the acceptor complex. The ionization potential (IP) and electron affinity (EA) were estimated as follows: $IP = E^{C}_{c} - E^{N}_{n}$ and $EA = E^{N}_{n} - E^{A}_{a}$, where the subscript depicts the charge state (neutral, cation, or anion) and the superscript depicts the geometry of the optimized structure.[53]

The open circuit voltage (V_{OC}) of the compounds was evaluated using eqn (11):[53,54]

$$qV_{OC} = |E^{D}_{HOMO} - E^{A}_{LUMO}| - 0.3 \quad (11)$$

where E^{A}_{LUMO} refers to the LUMO of the acceptor molecule, and E^{D}_{HOMO} refers to the HOMO of the donor polymer. The value of 0.3 eV is commonly accepted as the energy loss attributed to energy disorder and charge recombination.[55] The non-radiative energy losses (E_{loss}) of the designed NFAs were estimated using eqn (12):[2]

$$E_{loss} = E_{OP} - eV_{OC} \quad (12)$$

Finally, the difference between the ground state and excited state dipole moments ($\Delta\mu$) was estimated by analyzing the variations in the dipole along each coordinate axis:

$$\Delta\mu = \sqrt{(\mu_{gx} - \mu_{ex})^2 + (\mu_{gy} - \mu_{ey})^2 + (\mu_{gz} - \mu_{ez})^2} \quad (13)$$

where μ_{gx}, μ_{gy}, and μ_{gz} define the ground state dipole moments along the x, y, and z directions, and μ_{ex}, μ_{ey}, and μ_{ez} represent the excited state dipole moments along the x, y, and z directions, respectively.

2.2 Material design strategy

Fig. 1 depicts the chemical structures of the symmetric and asymmetric NFAs designed in this study. Sixty NFAs were designed by alternating the terminal acceptor moieties linked with the core donor unit. We have chosen five distinct acceptors (A1–A5) and four distinct core donors (D1–D4), which can possess an acceptor–donor–acceptor type configuration, resulting in twenty symmetric NFAs with the same terminal units. Additionally, there are forty asymmetric NFAs in which the terminal units are different. The core donor and acceptor moieties selected in this study are derived from small-molecule acceptors, as cited in ref. 30–37, whose PCEs are within the range of 10.7–17.8%. Thus, these molecular building blocks are part of non-fullerene acceptors already synthesized experimentally. The A1 acceptor is formed by the functionalization of two chlorine atoms at the 1,1-dicyanomethylene-3-indanone terminal acceptor unit. Substituting two fluorine atoms instead of chlorine atoms yielded the A2 acceptor. Elongation of the conjugation length in terms of adding one more phenyl ring in A1 results in the formation of the A3

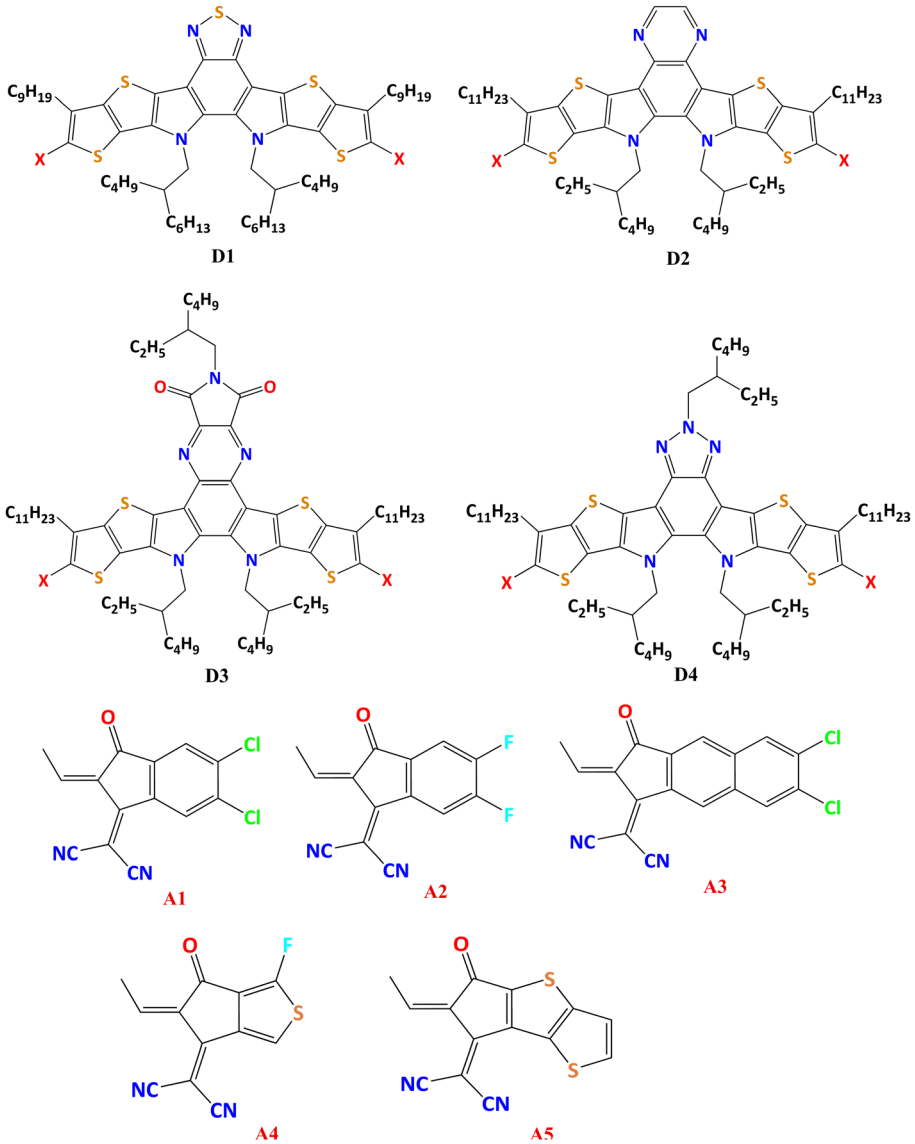

Fig. 1 Chemical structures of the building blocks and terminal acceptor (A1–A5) and core donor (D1–D4) units used in this study to design symmetric and asymmetric non-fullerene acceptor molecules.

acceptor. Similarly, the A4 acceptor is formed when the phenyl ring of the 1,1-dicyanomethylene-3-indanone terminal unit is replaced with a fluorinated thiophene group. Elongation by one more thiophene ring and the removal of the fluorine atom in A4 result in the formation of the A5 acceptor.

3 Results and discussion

3.1 Energy levels and photovoltaic properties

The chemical structure (top view) and frontier molecular orbital pictures (side view) of the symmetric and asymmetric donor/acceptor complexes are illustrated in Fig. S1 of the ESI.† As seen from Fig. S1 of the ESI,† both symmetric and asymmetric complexes, when coupled with the PM6 donor, exhibit a comparable π-stacking pattern. Furthermore, the frontier molecular orbital confirms the presence of distinct molecular orbitals, with HOMOs predominantly localized in the donor and LUMOs concentrated in the acceptor part. Our primary objective is to elucidate a correlation between symmetrically and asymmetrically functionalized small molecule acceptors to identify potential candidates for organic solar cells.

Electrostatic potential (ESP) surface maps of the core donor D1 and terminal acceptors A1–A5 are shown in Fig. S2 of the ESI.† The ESP maps offer insights into the surface charge distribution within the molecule, indicating regions assigned with positive, negative, and neutral charges. In the regions denoted with a higher ESP, electrons tend to accumulate more readily, fostering efficient charge separation and facilitating the formation of charge-transfer complexes.[56,57] This localized charge distribution influences the current density by affecting the rate of charge carrier transport through the NFA material.

Furthermore, the potential gradients between the donor and acceptor units determine the driving force for charge separation, thereby impacting the open-circuit voltage of the solar cell. The regions with positive ESP, represented by the mint color, appear in the central core of the π-conjugated system. However, the negative ESP (mapped with pink color) is centered on the –CN and –O groups present at the terminal acceptor. Fig. S2 of the ESI† shows that all fifteen complexes' negative ESP appears similar, attributed to the presence of the –CN and –O groups in the terminal acceptor units. In contrast, the positive ESP surface density distribution varies slightly from one system to another due to the presence of different terminal acceptor units. Our electrostatic potential analysis demonstrated a variation in the electron density within the molecules, attributed to the presence of electron-rich and electron-deficient units.

Table S2 in the ESI† provides a comprehensive overview of the investigated systems' computed electronic and photovoltaic properties. The energy gap (Δ_{LUMO}) between the LUMO and the LUMO+1 level, as outlined in Table S2 (ESI†), is consistently below 0.3 eV, accompanied by an exciton binding energy below 0.36 eV for the examined non-fullerene acceptors. According to Kuzmich *et al.*,[58] a small Δ_{LUMO}, combined with a sufficiently low-lying LUMO+1 level in the acceptor, increases the likelihood of electron acceptance from the donor's LUMO, thereby enhancing the power conversion efficiency of the device. Table S2 (ESI†) reveals that the combination of the terminal A5 moiety with various acceptor and core moieties consistently yields lower Δ_{LUMO} values compared to other combinations. Additionally, symmetrically functionalized terminal acceptor A5-based compounds (A5–D1–A5, A5–D2–A5, A5–D3–A5, and A5–D4–A5) exhibit Δ_{LUMO} in the range of 0.13–0.15 eV, representing the lowest values among the designed compounds. Notably, the absorption wavelength (λ_{max}) of the designed compounds falls within the visible spectrum (687–769 nm) with a relatively high oscillator strength (1.527 to 2.307), indicating a bright S_1 state in these systems. The computed oscillator strengths of these complexes are tabulated in Table S2 of the ESI.† Fusion of terminal acceptors with the D4 core donor demonstrates a higher absorption wavelength exceeding 730 nm, corresponding to an oscillator strength greater than 1.575, resulting in a bathochromic shift compared to other combinations. In the D4 core, the adjacent electron-rich donor (thiophene unit) and electron-deficient acceptor (benzotriazole unit) are chemically bonded in a coplanar fused D–A structure, enhancing electronic interactions between the donor and acceptor units.[59,60] The benzotriazole core, characterized by its fused 5-membered ring with three nitrogen atoms, stands out for its remarkable ability to induce a red shift in the absorption spectra compared to the other three cores, benzothiazole (D1), quinoxaline (D2), and quinoxalineimide (D3), fused with the thienylthiophene unit. Moreover, the complexes based on the D4 core exhibit a relatively lower HOMO–LUMO gap (1.973 to 2.039 eV) than that of complexes linked with other cores, D1–D3 (1.975 to 2.169 eV). Incorporating the N–N–N group (D4 core) within the fused ring system enhances electron delocalization and stabilizes the excited state. As a result, the reduced energy gap in D4-linked complexes facilitates tuning of the absorption wavelength towards a bathochromic shift, falling within the wavelength range of 730–769 nm. Among all complexes, the symmetrical complex A3–D4–A3 exhibits the maximum wavelength (λ_{max} = 769 nm) associated with an oscillator strength of 2.21. Furthermore, the elongation of the conjugation length (presence of maximum units of hexagonal rings) in the A3 terminal group contributes to the increase in wavelength compared to other complexes. In contrast, most D1–D3 core-linked NFAs fall within the visible wavelength region below 730 nm.

The open-circuit voltage, a crucial parameter influencing the material efficiency and overall organic solar cell performance, was estimated in the presence of a PM6 polymer. The estimated device performance is summarized in Table S2 of the ESI† (additional excel sheet). As can be seen from Table S2 (ESI†), V_{OC} values for the examined NFAs range from 1.2 to 1.7 V. According to Liu *et al.*,[26] the thiophene-based terminal acceptor moieties A4 and A5 tend to enhance the V_{OC}. In contrast, A1–A3 terminal acceptors are more favorable for improving the short-circuit current. Remarkably, except for a few systems, A4 and A5 terminal unit-based symmetric and asymmetric NFAs exhibit V_{OC} values over 1.4 V, attributed to fused thiophene rings in the terminal units. Conversely, the remaining NFAs exhibit a V_{OC} below 1.4 V. The designed symmetric and asymmetric NFAs, characterized by a lower exciton binding energy (<0.36 eV), a small Δ_{LUMO}, and a larger V_{OC}, are anticipated to enhance the solar cell characteristics and improve the device performance. Acceptors with A5 as one of the terminals possess slightly higher LUMO energy levels (less negative) than their counterparts (see Table S2, ESI†). It is evident from eqn (11) that the magnitude of V_{OC} tends to increase as the LUMO energy of the acceptor becomes high (less negative number). Due to this reason, A5 terminal-based acceptors possess the highest V_{OC} among all the studied complexes.

3.2 Charge separation/recombination *versus* dipole moment

Fig. 2 presents a correlation plot illustrating the relationship between the free energy associated with charge separation (ΔG_{CS}) and that for charge recombination (ΔG_{CR}) and the difference between the ground state and excited dipole moments ($\Delta\mu$). As described by Liu *et al.*,[61] a higher $\Delta\mu$, indicative of a robust intramolecular charge transfer effect, enhances exciton dissociation and charge generation efficiencies, leading to improved photovoltaic performance. Fig. 2 shows that an increase in $\Delta\mu$ correlates with an increase in ΔG_{CS}, while ΔG_{CR} follows a trend opposite to that of ΔG_{CS}. Specifically, higher values of ΔG_{CS} and lower values of ΔG_{CR} are crucial for achieving enhanced charge separation and reduced recombination rates. Notably, symmetric and asymmetric NFAs functionalized with the A5 terminal moiety and D1, D2, and D4 π-core units exhibit $\Delta\mu$ greater than 1.0 Dy, suggesting improved intramolecular charge transfer properties within these systems. In contrast, the remaining compounds, incorporating acceptor units (A1–A4) and cores (D1, D2, and D4), demonstrate $\Delta\mu$ values below 1.0 Dy, contributing to the decreased ΔG_{CS}. Fig. 2 highlights that most D3 core-linked symmetric and asymmetric acceptors possess $\Delta\mu$ (>1.5 Dy)

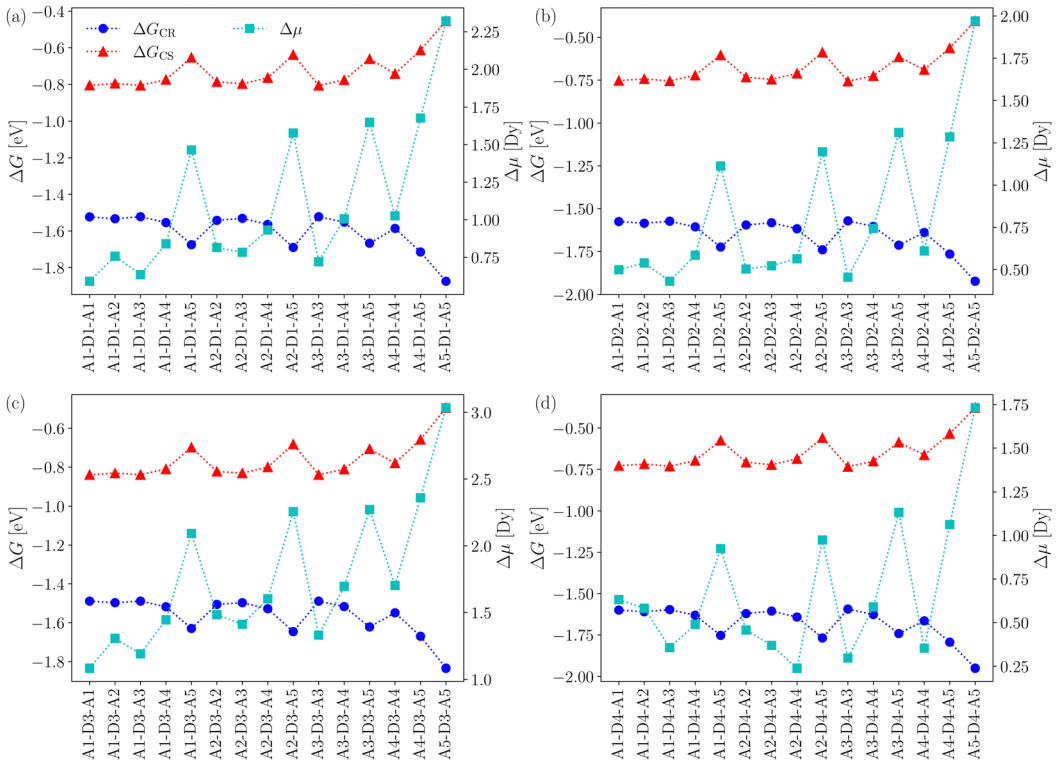

Fig. 2 Variation in ΔG_{CS} and ΔG_{CR} along with the difference in dipole moments between ground and excited states as a function of terminal acceptor units for a fixed core donor (D1–D4) in the investigated non-fullerene acceptor molecules: (a–d) D1–D4 core donor functionalized complexes.

significantly higher than those of other systems. This difference can be attributed to the pentagonal imide functional group fused with a pyrazine aromatic ring in the core unit, extending the π-conjugation length and influencing the performance. As discussed in ref. 62 and 63, the elongation of conjugation length plays a pivotal role in reducing the molecular symmetry and planarity, enhancing both the dipole moment and solubility.

Symmetric and asymmetric NFAs functionalized with D1–D4 core units and A5 terminal acceptors exhibit lower ΔG_{CR} (<-1.6 eV) and larger ΔG_{CS} (>-0.7 eV) values, suggesting improved charge separation rates and overall solar cell performance. These compounds also exhibit higher $\Delta\mu$ values exceeding 1.0 Dy. Further analysis, as shown in Fig. 2, reveals that variations in acceptors from A1 to A5, with A1 fixed at one end, result in higher $\Delta\mu$ values and increased ΔG_{CS}, while ΔG_{CR} decreases inversely. NFAs functionalized with A4 and A5 at one end and the A1 acceptor at the other end with the same D1 core units exhibit higher ΔG_{CS} and $\Delta\mu$ values, attributed to the presence of the conjugated thiophene ring at the terminal units. Additionally, due to the elongation of π-conjugation in A3 compared to that of A1, increased ΔG_{CS} and $\Delta\mu$ were obtained in the case of A1–D1–A3 compared to those of A1–D1–A1. Moreover, the fluorinated terminal acceptor A2 outperforms A1 and A3 in terms of superior ΔG_{CS} and $\Delta\mu$ values, as seen in A1–D1–A2 *versus* A1–D1–A1 and A1–D1–A3. Furthermore, symmetric and asymmetric acceptors functionalized with A3 at one end and A3–A5 at the other end, with the same core D1, exhibit a trend similar to A1- and A2-functionalized complexes combined with core D1. Overall, A5–D1–A5 symmetric acceptors show maximum ΔG_{CS} and $\Delta\mu$ values compared to their symmetric or asymmetric counterparts. Similar correlations are observed for the D2–D4 core functionalized with A1–A5 terminal acceptor units, maintaining consistent energy trends across the complexes. Despite slight changes in the computed values, the overall trends concerning ΔG_{CS}, ΔG_{CR}, and $\Delta\mu$ remain consistent throughout the examined complexes.

We have further estimated the charge separation (k_{CS}) and recombination (k_{CR}) rates in the examined NFAs. The variation in these rates, along with $\Delta\mu$, as a function of terminal acceptor functionalization for a fixed core donor unit is shown in Fig. S3 of the ESI.† As observed, k_{CS} exhibits a direct correlation with $\Delta\mu$, while k_{CR} shows an inverse correlation as $\Delta\mu$ increases. This pattern mirrors the trends observed in the free energy-dipole moment correlation, as shown in Fig. 2. Most non-fullerene acceptors demonstrate k_{CS} in the order of 10^{15} s^{-1}, with a few falling within 10^{14} s^{-1}. Notably, A1–D4–A5 and A4–D4–A5, both asymmetric compounds with fused aromatic N–N–N core units, exhibit an exceptionally high k_{CS} in the order of 10^{16} s^{-1}. Overall, A5-linked symmetric and asymmetric NFAs display k_{CR} values below 10^4 s^{-1}, notably lower than the maximum value of approximately 10^6 s^{-1}, emphasizing their higher k_{CS} rates. In A4-linked complexes, k_{CR} is more than two orders of magnitude higher than that of their A5-linked counterparts, although still one order of magnitude lower than A1–A3-linked complexes. These variations in k_{CS} and k_{CR} are attributed to diverse core donor and terminal acceptor unit functionalizations. Furthermore, Fig. S3

(ESI†) highlights that the functionalization of high open-circuit voltage (V_{OC}) based A4 and A5 terminal units contributes to reduced k_{CR} and substantially increased $\Delta\mu$ values. The considerable enhancement in k_{CR} rates negatively correlates with $\Delta\mu$, underscoring the significance of $\Delta\mu$ as a crucial parameter in determining potential materials for organic solar cells.

3.3 Charge separation/recombination *versus* energy loss

The non-radiative energy losses of the designed NFA molecules were evaluated using eqn (12), aligning with Yan *et al.*'s suggestion[2] that minimizing deviations between the V_{OC} and optical excitation energy (E_{OP}) could identify promising materials for organic solar cells. Fig. 3 shows a three-color point plot, where red, blue, and green denote ΔG_{CS}, ΔG_{CR}, and E_{loss} for symmetric and asymmetric complexes, respectively. In Fig. S4 of the ESI,† a similar plot illustrates the variation in charge separation and recombination rates along with energy losses for both complex types. A consistent reduction in ΔG_{CR} is observed with decreasing E_{loss}, while ΔG_{CS} exhibits a negative correlation with E_{loss}. A decrease in E_{loss} corresponds to a higher energy value (negative) of ΔG_{CS}. Solar cell parameters, including E_{loss}, ΔG_{CS}, ΔG_{CR}, k_{CS}, and k_{CR}, are summarized in Table S2 of the ESI.† The top panel of Fig. 3 shows that E_{loss} decreases as ΔG_{CS} increases, moving from A1–D1–A1 to A1–D1–A5, with an inverse trend in ΔG_{CR}. A similar trend is observed for other terminal acceptor moieties, *i.e.*, symmetric and asymmetric acceptors with A4 and A5 terminals consistently exhibit lower energy losses. These complexes, featured in Fig. 2, demonstrate notably higher $\Delta\mu$ values compared to others. It is important to note that similar trends are valid when the central core unit is changed from D1 to D2, D3, or D4. However, the variation in energy values is prominent due to distinct core donor units (D1–D4). As can be seen from Table S2 (ESI†), A5-linked symmetric and asymmetric complexes consistently maintain an E_{loss} below 0.35 eV, enriching ΔG_{CS} and k_{CS} rates. Furthermore, the bottom panel of Fig. 3 and Fig. S4 of the ESI† indicate that D3 core-linked complexes (except for A5 linked D3 complexes) exhibit E_{loss} values exceeding 0.4 eV. This rise in energy losses contributes to a one-order magnitude reduction in k_{CS} compared to other complexes, leading to a one-order magnitude increase in k_{CR}. Furthermore, Fig. S5 of the ESI† depicts an inverse correlation between E_{loss} and $\Delta\mu$. Except for D3-functionalized complexes, all D1, D2, and D4 functionalized complexes fall below the E_{loss} threshold of 0.4 eV, denoting substantial $\Delta\mu$. Elevated E_{loss} values in D3-functionalized complexes may adversely affect the solar cell performance, emphasizing E_{loss} as a critical parameter for identifying potential NFA candidates.

3.4 Correlation heat map ratio plots

As reported by Luo *et al.*, the PCE of the asymmetric BTP-2ThCl is significantly enhanced compared to those of the symmetric compounds BTP-4F and BTP-2ThCl. A balanced value for V_{OC} and J_{SC} was observed in the BTP-2ThCl compound, which falls in between the values of the BTP-4F and BTP-2ThCl compounds, respectively.[29] For instance, a similar pattern of results

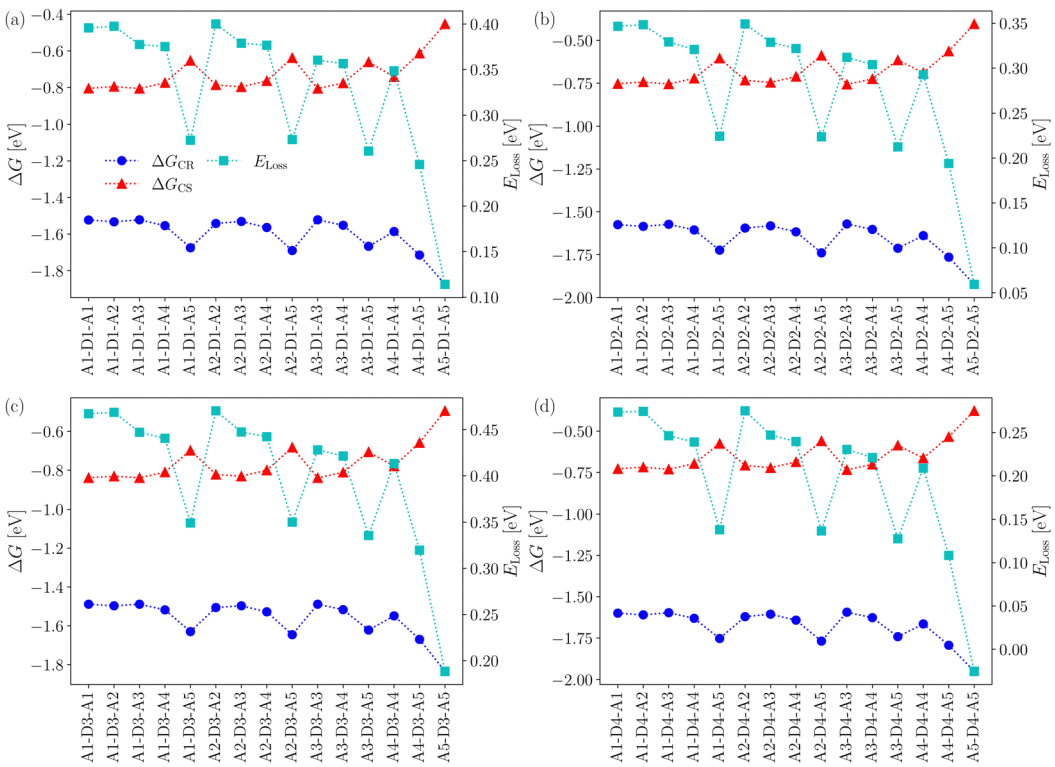

Fig. 3 Variation in ΔG_{CS} and ΔG_{CR} along with the non-radiative energy loss (E_{loss}) as a function of terminal acceptor units for a fixed core donor (D1–D4) in the investigated non-fullerene acceptor molecules: (a–d) D1–D4 core donor functionalized complxes.

is also observed in our investigation when comparing the asymmetric compound A1–D1–A2 with the symmetric compounds A1–D1–A1 and A2–D1–A2. The computed values of V_{OC} and λ_{max} for the asymmetric compound A1–D1–A2 are found to be 1.307 V and 727.4 nm, respectively, falling between the values for A1–D1–A1 (V_{OC} = 1.298 V and λ_{max} = 731.1 nm) and A2–D1–A2 (V_{OC} = 1.316 V and λ_{max} = 722.6 nm). Furthermore, we have observed balanced E_b, Δ_{LUMO} and $\Delta\mu$ values of the A1–D1–A2 complex falling in between two symmetrical acceptors A1–D1–A1 and A2–D1–A2, which is confirmed by the previous study report by Luo *et al.*[29] In order to gain a comprehensive understanding of how alterations in the end-group acceptors (A1–A5) impact the rates and free energies, we investigate a set of heat map plots that depict the ratios of rates and free energies associated with specific core units (D1–D4). The heat map plot of the ratio between k_{CS} and k_{CR} with respect to four different cores (D1–D4) is illustrated in Fig. 4. A similar correlation plot of the ratio of ΔG_{CS} to ΔG_{CR} is depicted in Fig. S6 of the ESI.† Fig. 4 illustrates that efficient complexes can be selected based on their higher rate ratio values (ratio of k_{CS} to k_{CR}). In general, to observe such situations, the k_{CS} value should be higher than that of k_{CR}. As is evident from Fig. 4, it is noted that when each core unit is paired with the symmetric terminal acceptor A5, it results in the highest rate ratio (k_{CS}/k_{CR}) among all possible combinations. As cited in ref. 20, the terminal thiophene decorated small molecule acceptors displayed a high V_{OC} and contributed to improved overall performance. Therefore, the significant enhancement observed in the symmetric A5–D1–A5 compound can be attributed to the elongation of the fused thiophene rings within the terminal acceptor moiety, which significantly enhances the V_{OC} values as seen in our computed results summarized in Table S2 of the ESI.† Furthermore, efficiency in terms of rate ratio decreases substantially when moving from acceptor A5 to A1. A similar trend is also followed for the A1–A5 acceptors when paired with the remaining core donors D2–D4. Compared to the asymmetric compounds A1–D1–A5 and A3–D1–A5, the A2–D1–A5 and A4–D1–A5 compounds displayed a higher rate ratio. It is important to note that when the higher V_{OC} based terminal units A4 and A5 are fuzed with the higher J_{SC} based A2 terminal unit, they yield better rate ratio values than other systems. This observation further substantiates the experimental results reported in ref. 64 that in conjugation with a J71 polymer, the A1 functionalized NTTIC-Cl (10.8%) complex achieved lower power conversion efficiencies than those of the A2 functionalized NTTIC-F (11%) compound. However, it is worth noting that the NTTIC-Cl complex exhibited a slightly higher J_{SC} as compared to the NTTIC-F compound. Furthermore, elongation of the conjugation length within the A3 unit leads to an increase in wavelength and a rise in Δ_{LUMO}, while significantly decreasing the V_{OC} value when comparing the A3–D1–A5 complex with A1–D1–A5, A2–D1–A5, and A4–D1–A5.

Fig. 4b–d shows a similar pattern to Fig. 4a when core units D2–D4 are paired with A1–A5 terminal moieties. Moreover, the core unit D4 fuzed with symmetric and asymmetric A5 acceptors exhibited a higher rate ratio than those of D1, D2, and D3 substituted compounds. The rate ratio follows the order A5–D4–A5 > A5–D2–A5 > A5–D1–A5 > A5–D3–A5. As is evident from Table S2 of the ESI,† the functionalization of the imide group on the core unit D3 enhances $\Delta\mu$ and increases both E_{loss} and E_b while decreasing the V_{OC} compared to D2 and D1. The increase in E_{loss} and E_b and the decrease in V_{OC} affect their rate

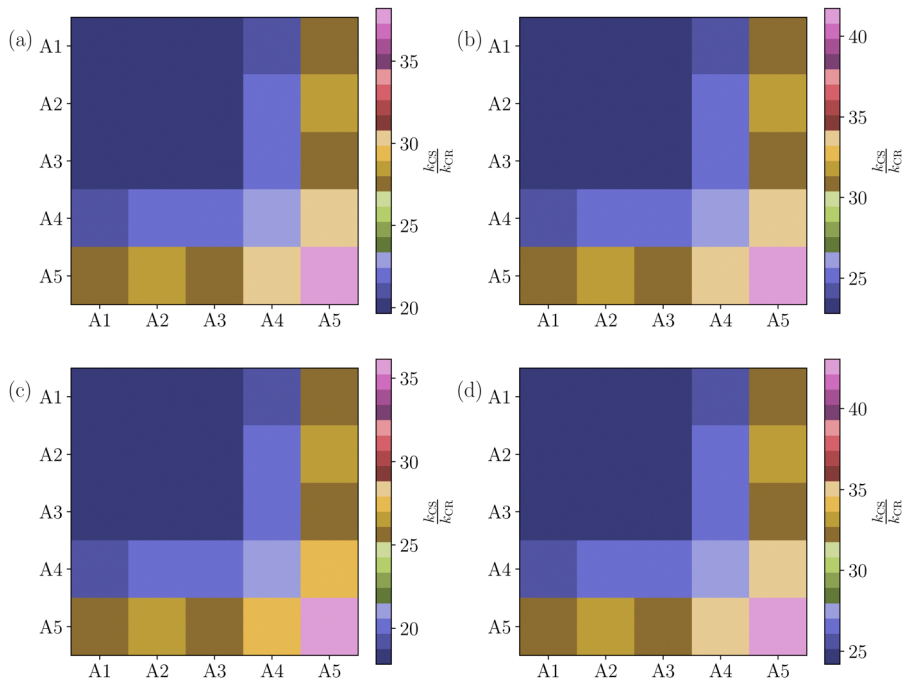

Fig. 4 Heat map plot of the ratio between k_{CS} and k_{CR} with respect to four different cores (D1–D4). The color of each point represents the acceptor moiety of the complex: (a–d) D1–D4 core donor functionalized complexes.

ratio value. Among all the complexes, the D4-linked acceptor displayed an improved rate ratio, attributed to the functionalization of the core unit with the N–N–N functional group. Following the A5 terminal acceptor group, symmetric complexes arising from a combination between A4 and donor cores D1–D4 exhibit the best rate ratio values, as illustrated in Fig. 4. The efficiency decreases as it moves towards the A3, A2, and A1 terminal units, as visualized in the heat map plots. From the above analysis, we can conclude that the symmetric and asymmetric small molecule acceptors, especially those associated with the A5 terminal group, consistently yield favorable results compared to other compounds. More importantly, it is not always true that an asymmetric combination yields better results than its symmetric counterparts. Instead, the overall A–D–A architecture determines the efficiency of a non-fullerene acceptor molecule.

4 Conclusions

In this study, we comprehensively analyzed symmetric and asymmetric non-fullerene small molecule acceptors in conjunction with the PM6 donor polymer, utilizing first-principle simulations to estimate their solar cell properties. The focus of our investigation was the design of A–D–A-type frameworks, strategically combining high short-circuit current (J_{SC}) and high open-circuit voltage (V_{OC}) based terminal acceptor moieties with various central donor units. In contrast to the common belief that modifying from symmetric to asymmetric compounds consistently enhances their potential for organic solar cells, our findings emphasize that such a transition does not always yield favorable outcomes. Importantly, our designed small molecule acceptors consistently exhibit lower values of the difference in the lowest unoccupied molecular orbital ($\Delta_{LUMO} < 0.3$ eV), exciton binding energy ($E_b < 0.36$ eV), and V_{OC} ranging between approximately 1.2 and 1.7 V. Notably, configurations involving the A5 acceptor at one end and A1–A5 acceptors linking at the other end in symmetric and asymmetric non-fullerene acceptors display significant enhancements in $\Delta\mu$ and charge separation rates (k_{CS}) and lower energy losses ($E_{loss} < 0.35$ eV). This design strategy provides a clear and insightful guide for researchers aiming to develop next-generation small-molecule acceptors for efficient organic solar cells.

Author contributions

AM and RK conceived the problem. RK conducted all the simulations. AM and RK analyzed the results and prepared the draft.

Conflicts of interest

There are no conflicts to declare.

Acknowledgements

The authors gratefully acknowledge the Indian Institute of Technology Gandhinagar, India, for providing research facilities and financial support. AM acknowledges the SERB (SRG/2022/001532) project for funding. RK and AM are grateful to PARAM Ananta for computational resources.

Notes and references

1 P. Cheng, G. Li, X. Zhan and Y. Yang, *Nat. Photonics*, 2018, **12**, 131–142.
2 C. Yan, S. Barlow, Z. Wang, H. Yan, A. K.-Y. Jen, S. R. Marder and X. Zhan, *Nat. Rev. Mater.*, 2018, **3**, 1–19.
3 A. Markina, K.-H. Lin, W. Liu, C. Poelking, Y. Firdaus, D. R. Villalva, J. I. Khan, S. H. Paleti, G. T. Harrison and J. Gorenflot, *et al.*, *Adv. Energy Mater.*, 2021, **11**, 2102363.
4 J. Hou, O. Inganäs, R. H. Friend and F. Gao, *Nat. Mater.*, 2018, **17**, 119–128.
5 D. Luo, W. Jang, D. D. Babu, M. S. Kim, D. H. Wang and A. K. K. Kyaw, *J. Mater. Chem. A*, 2022, **10**, 3255–3295.
6 T. Yang, L. Gao, J. Lu, C. Ma, Y. Du, P. Wang, Z. Ding, S. Wang, P. Xu and D. Liu, *et al.*, *Nat. Commun.*, 2023, **14**, 839.
7 H. Min, D. Y. Lee, J. Kim, G. Kim, K. S. Lee, J. Kim, M. J. Paik, Y. K. Kim, K. S. Kim and M. G. Kim, *et al.*, *Nature*, 2021, **598**, 444–450.
8 J. Fu, P. W. Fong, H. Liu, C.-S. Huang, X. Lu, S. Lu, M. Abdelsamie, T. Kodalle, C. M. Sutter-Fella and Y. Yang, *et al.*, *Nat. Commun.*, 2023, **14**, 1760.
9 K. Liu, Y. Jiang, F. Liu, G. Ran, F. Huang, W. Wang, W. Zhang, C. Zhang, J. Hou and X. Zhu, *Adv. Mater.*, 2023, **35**, 2300363.
10 Z. Chen, J. Zhu, D. Yang, W. Song, J. Shi, J. Ge, Y. Guo, X. Tong, F. Chen and Z. Ge, *Energy Environ. Sci.*, 2023, **16**, 3119–3127.
11 M. Ans, K. Ayub, I. A. Bhatti and J. Iqbal, *RSC Adv.*, 2019, **9**, 3605–3617.
12 M. Ans, J. Iqbal, I. A. Bhatti and K. Ayub, *RSC Adv.*, 2019, **9**, 34496–34505.
13 M. Ans, K. Ayub, S. Muhammad and J. Iqbal, *Comput. Theor. Chem.*, 2019, **1161**, 26–38.
14 J. Yang, W.-L. Ding, Q.-S. Li and Z.-S. Li, *J. Phys. Chem. Lett.*, 2022, **13**, 916–922.
15 J. Yang, W.-L. Ding, Q.-S. Li and Z.-S. Li, *Molecules*, 2023, **28**, 811.
16 Z. Zhang, D. Li, H. Zhang, X. Ma, Y.-N. Chen, A. Zhang, X. Xu, Y. Liu, Z. Ma and Z. Bo, *J. Mater. Chem. C*, 2022, **10**, 2792–2799.
17 C. Li, T. Xia, J. Song, H. Fu, H. S. Ryu, K. Weng, L. Ye, H. Y. Woo and Y. Sun, *J. Mater. Chem. A*, 2019, **7**, 1435–1441.
18 T. Liu, Y. Zhang, Y. Shao, R. Ma, Z. Luo, Y. Xiao, T. Yang, X. Lu, Z. Yuan and H. Yan, *et al.*, *Adv. Funct. Mater.*, 2020, **30**, 2000456.
19 P. Gopikrishna, H. Choi, D. H. Kim, J. H. Hwang, Y. Lee, H. Jung, G. Yu, T. B. Raju, E. Lee and Y. Lee, *et al.*, *Chem. Sci.*, 2021, **12**, 14083–14097.

20 T. Liu, H. Zheng, X. Yu, S. Shi and Y. Zhou, *et al.*, *J. Mater. Chem. C*, 2023, **11**, 5257–5270.
21 D. Li, C. Sun, T. Yan, J. Yuan and Y. Zou, *ACS Cent. Sci.*, 2021, **7**, 1787–1797.
22 J. Yang, Q.-S. Li and Z.-S. Li, *Phys. Chem. Chem. Phys.*, 2021, **23**, 12321–12328.
23 Y. Chen, H. Meng, L. Ding, J. Tang, J. Yi, J. Zhang, Z. Wang, R. Ma, Z. Li and L. Lyu, *et al.*, *Chem. Mater.*, 2022, **34**, 10144–10152.
24 L. Xie, A. Lan, Q. Gu, S. Yang, W. Song, J. Ge, R. Zhou, Z. Chen, J. Zhang and X. Zhang, *et al.*, *ACS Energy Lett.*, 2022, **8**, 361–371.
25 C. Li, H. Fu, T. Xia and Y. Sun, *Adv. Energy Mater.*, 2019, **9**, 1900999.
26 T. Liu, H. Zheng, X. Yu, S. Shi and Y. Zhou, *et al.*, *J. Mater. Chem. C*, 2023, **11**, 5257–5270.
27 L. Ye, Y. Xie, Y. Xiao, J. Song, C. Li, H. Fu, K. Weng, X. Lu, S. Tan and Y. Sun, *J. Mater. Chem. A*, 2019, **7**, 8055–8060.
28 M. Li, Y. Zhou, J. Zhang, J. Song and Z. Bo, *J. Mater. Chem. A*, 2019, **7**, 8889–8896.
29 Z. Luo, R. Ma, T. Liu, J. Yu, Y. Xiao, R. Sun, G. Xie, J. Yuan, Y. Chen and K. Chen, *et al.*, *Joule*, 2020, **4**, 1236–1247.
30 X. Duan, W. Song, J. Qiao, X. Li, Y. Cai, H. Wu, J. Zhang, X. Hao, Z. Tang and Z. Ge, *et al.*, *Energy Environ. Sci.*, 2022, **15**, 1563–1572.
31 Z. Zhou, W. Liu, G. Zhou, M. Zhang, D. Qian, J. Zhang, S. Chen, S. Xu, C. Yang and F. Gao, *et al.*, *Adv. Mater.*, 2020, **32**, 1906324.
32 C. Zhu, K. An, W. Zhong, Z. Li, Y. Qian, X. Su and L. Ying, *Chem. Commun.*, 2020, **56**, 4700–4703.
33 S. Liu, J. Yuan, W. Deng, M. Luo, Y. Xie, Q. Liang, Y. Zou, Z. He, H. Wu and Y. Cao, *Nat. Photonics*, 2020, **14**, 300–305.
34 S. M. Swick, J. M. Alzola, V. K. Sangwan, S. H. Amsterdam, W. Zhu, L. O. Jones, N. Powers-Riggs, A. Facchetti, K. L. Kohlstedt and G. C. Schatz, *et al.*, *Adv. Energy Mater.*, 2020, **10**, 2000635.
35 X. Li, M.-A. Pan, T.-K. Lau, W. Liu, K. Li, N. Yao, F. Shen, S. Huo, F. Zhang and Y. Wu, *et al.*, *Chem. Mater.*, 2020, **32**, 5182–5191.
36 M. Deng, X. Xu, Y. W. Lee, L. K. Ericsson, E. Moons, H. Y. Woo, Y. Li, L. Yu and Q. Peng, *Nanoscale*, 2020, **12**, 12928–12941.
37 M. Li, Z. Li, G. Song, C. Jiang, X. Chen, J. Wang, Y. Yang, X. Wan, C. Li and Y. Chen, *J. Mater. Chem. C*, 2023, **11**, 1155–1164.
38 Y. Zhao and D. G. Truhlar, *Theor. Chem. Acc.*, 2008, **120**, 215–241.
39 T. Yanai, D. P. Tew and N. C. Handy, *Chem. Phys. Lett.*, 2004, **393**, 51–57.
40 M. Ans, J. Iqbal, B. Eliasson, M. J. Saif, H. M. A. Javed and K. Ayub, *J. Mol. Model.*, 2019, **25**, 1–12.
41 M. Ans, M. Paramasivam, K. Ayub, R. Ludwig, M. Zahid, X. Xiao and J. Iqbal, *J. Mol. Liq.*, 2020, **305**, 112829.
42 S. Grimme, J. Antony, S. Ehrlich and H. Krieg, *J. Chem. Phys.*, 2010, **132**, 154104.
43 F. Weigend and R. Ahlrichs, *Phys. Chem. Chem. Phys.*, 2005, **7**, 3297–3305.
44 M. J. Frisch *et al.*, *Gaussian 09 Revision E.01*, Gaussian Inc., Wallingford CT, 2009.
45 F. Neese, *Wiley Interdiscip. Rev.: Comput. Mol. Sci.*, 2012, **2**, 73–78.
46 P. Pracht, F. Bohle and S. Grimme, *Phys. Chem. Chem. Phys.*, 2020, **22**, 7169–7192.
47 S. Grimme, *J. Chem. Theory Comput.*, 2019, **15**, 2847–2862.
48 R. A. Marcus, *J. Chem. Phys.*, 1956, **24**, 966–978.
49 E. F. Valeev, V. Coropceanu, D. A. da Silva Filho, S. Salman and J.-L. Brédas, *J. Am. Chem. Soc.*, 2006, **128**, 9882–9886.
50 Y. Li, T. Pullerits, M. Zhao and M. Sun, *J. Phys. Chem. C*, 2011, **115**, 21865–21873.
51 S. Haseena and M. K. Ravva, *Sci. Rep.*, 2022, **12**, 15043.
52 R. Khatua and A. Mondal, *Mater. Adv.*, 2023, **4**, 4425–4435.
53 R. Khatua, B. Das and A. Mondal, *Phys. Chem. Chem. Phys.*, 2023, **25**, 7994–8004.
54 M. C. Scharber, D. Mühlbacher, M. Koppe, P. Denk, C. Waldauf, A. J. Heeger and C. J. Brabec, *Adv. Mater.*, 2006, **18**, 789–794.
55 M.-H. Lee, *Sol. Energy*, 2022, **234**, 360–367.
56 Y. Cui, P. Zhu, H. Hu, X. Xia, X. Lu, S. Yu, H. Tempeld, R.-A. Eichel, X. Liao and Y. Chen, *Angew. Chem.*, 2023, **135**, e202304931.
57 F. Cheng, Y. Cui, F. Ding, Z. Chen, Q. Xie, X. Xia, P. Zhu, X. Lu, H. Zhu and X. Liao, *et al.*, *Adv. Mater.*, 2023, **35**, 2300820.
58 A. Kuzmich, D. Padula, H. Ma and A. Troisi, *Energy Environ. Sci.*, 2017, **10**, 395–401.
59 L. Feng, J. Yuan, Z. Zhang, H. Peng, Z.-G. Zhang, S. Xu, Y. Liu, Y. Li and Y. Zou, *ACS Appl. Mater. Interfaces*, 2017, **9**, 31985–31992.
60 J.-S. Ni, Y.-C. Yen and J. T. Lin, *Chem. Commun.*, 2015, **51**, 17080–17083.
61 X. Ji, T. Wang, Q. Fu, D. Liu, Z. Wu, M. Zhang, H. Y. Woo and Y. Liu, *Macromol. Rapid Commun.*, 2023, **44**, 2300213.
62 B. Kan, H. Feng, X. Wan, F. Liu, X. Ke, Y. Wang, Y. Wang, H. Zhang, C. Li and J. Hou, *et al.*, *J. Am. Chem. Soc.*, 2017, **139**, 4929–4934.
63 U. Ali, A. Javed, H. Ramzan, M. Shoaib, A. Raza, M. T. Khalil, S.-B. Cheng and J. Iqbal, *Spectrochim. Acta, Part A*, 2020, **228**, 117685.
64 T. Umeyama, T. Wada, K. Igarashi, K. Kato, A. Yamakata, T. Takeyama, Y. Sakamoto, Y. Tamai, H. Ohkita and K. Ishida, *et al.*, *ACS Appl. Energy Mater.*, 2021, **4**, 14022–14033.

